HOLOGIC®
The Science of Sure

Powerful images.
Clear answers.

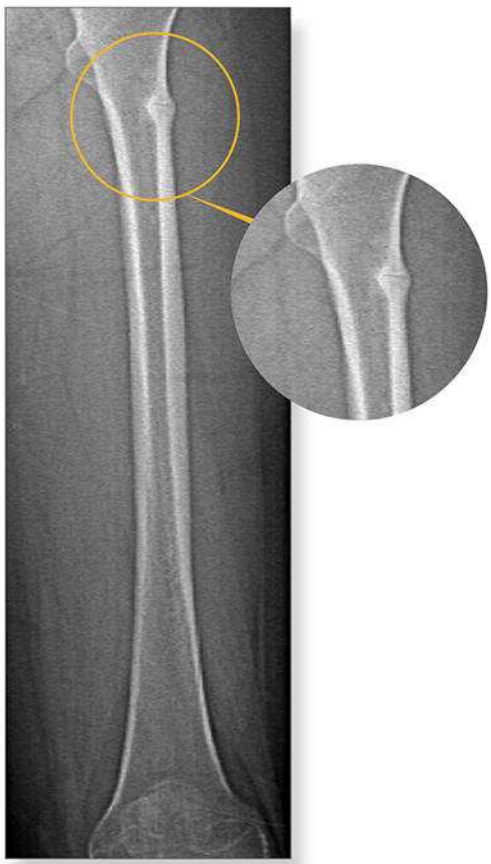

Manage Patient's concerns about Atypical Femur Fracture*

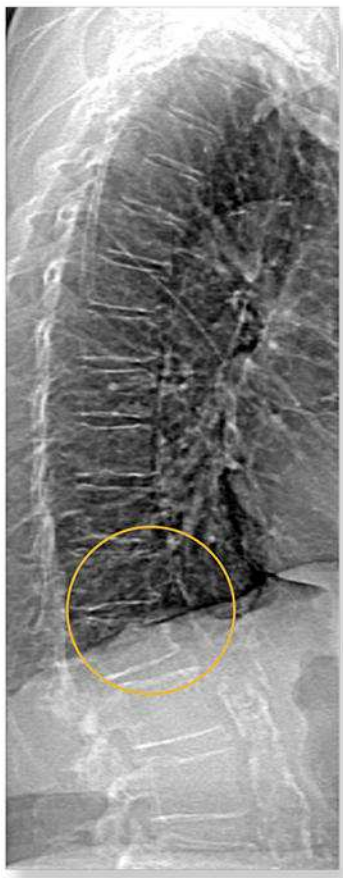

Vertebral Fracture Assessment – a critical part of a complete fracture risk assessment

Advanced Body Composition® Assessment – the power to see what's inside

Contact your Hologic rep today at insidesales@hologic.com

*Incomplete Atypical Femur Fractures imaged with a Hologic densitometer, courtesy of Prof. Cheung, University of Toronto

www.hologic.com | info@hologic.com | 1.781.999.7300

ORIGINAL ARTICLE

JBMR®

Inhibition of SLC7A11 by Sulfasalazine Enhances Osteogenic Differentiation of Mesenchymal Stem Cells by Modulating BMP2/4 Expression and Suppresses Bone Loss in Ovariectomized Mice

Chanyuan Jin,[1*] Ping Zhang,[1*] Min Zhang,[1] Xiao Zhang,[1] Longwei Lv,[1] Hao Liu,[1] Yunsong Liu,[1] and Yongsheng Zhou[1,2]

[1]Department of Prosthodontics, Peking University School and Hospital of Stomatology, Beijing, China
[2]National Engineering Lab for Digital and Material Technology of Stomatology, Peking University School and Hospital of Stomatology, Beijing, China

ABSTRACT

An imbalance in osteogenesis and adipogenesis is a crucial pathological factor in the development of osteoporosis. Many attempts have been made to develop drugs to prevent and treat this disease. In the present study, we investigated the phenomenon whereby downregulation of *SLC7A11* significantly enhanced the osteogenic differentiation of mesenchymal stem cells (MSCs) in vitro, and promoted the bone formation in vivo. Sulfasalazine (SAS), an inhibitor of SLC7A11, increased the osteogenic potential effectively. Mechanistically, inhibition of SLC7A11 by SAS treatment or knockdown of *SLC7A11* increased BMP2/4 expression dramatically. In addition, we detected increased *Slc7a11* expression in bone marrow MSCs of ovariectomized (OVX) mice. Remarkably, SAS treatment attenuated bone loss in ovariectomized mice. Together, our data suggested that SAS could be used to treat osteoporosis by enhancing osteogenic differentiation of MSCs. © 2016 American Society for Bone and Mineral Research.

KEY WORDS: SLC7A11; SULFASALAZINE; OSTEOGENIC DIFFERENTIATION; BONE MORPHOGENETIC PROTEIN; OSTEOPOROSIS

Introduction

Postmenopausal osteoporosis is caused primarily by estrogen deficiency after cessation of ovarian function, leading to architectural deterioration of bone structure, low bone mineral density, increased fragility, and susceptibility to fracture.[1] Previous studies suggested that these structural abnormalities are attributable to dysfunctional osteogenic differentiation of bone marrow-derived mesenchymal stem cells (MSCs), with a shift in lineage commitment and bone loss being accompanied by increased adipose tissues in the bone marrow.[2–4] The commitment and differentiation of MSCs toward an adipogenic or osteogenic cell fate depends on a variety of signaling and transcription factors. Among them, bone morphogenetic proteins (BMPs), especially BMP-2 and BMP-4, promote osteogenic commitment and terminal osteogenic differentiation in MSCs.[5,6] Small molecular compounds activating BMP2/4 expression might represent potential drugs to treat osteoporosis.

Cystine-glutamate antiporters are plasma membrane protein complexes that secrete glutamate and import cystine.[7–10] The functional core of these transporters is SLC7A11, also known as xCT, a predicted 12-transmembrane protein required for amino acid selectivity.[11–13] SLC7A11 is required for normal mammalian blood plasma redox homeostasis, skin pigmentation, immune system function, and memory formation.[14–16] Aberrant function of SLC7A11 is implicated in tumor growth and survival, cancer stem cell maintenance, drug resistance, and neurological dysfunction.[17–19] Recently, sulfasalazine (SAS) has emerged as an effective, clinically approved inhibitor of SLC7A11.[20] Historically, SAS, a pharmacological agent comprising a sulfa portion and a 5-ASA portion, was used based on the hypothesis that the drug provided two critical elements in the treatment of ulcerative colitis.[21] SAS was also used to treat rheumatoid arthritis long before it was used to treat patients with ulcerative colitis.[22,23] However, whether SLC7A11 and SAS play roles in the osteogenic differentiation of human MSCs (hMSCs) and osteoporosis treatment was unreported.

Herein, we report our investigation of the contribution of SLC7A11 to the osteogenic potential of MSCs. Our data indicates that *SLC7A11* silencing significantly increased the osteogenic potential of MSCs, both in vitro and in vivo. Moreover, we show that pharmacological inhibition of SLC7A11 by SAS enhanced

Received in original form April 20, 2016; revised form September 24, 2016; accepted September 29, 2016. Accepted manuscript online September 29, 2016.
Address correspondence to: Yongsheng Zhou, DDS, PhD, Department of Prosthodontics, Peking University School and Hospital of Stomatology, 22 Zhongguancun South Avenue, Haidian District, Beijing 100081, China. E-mail address: kqzhouysh@hsc.pku.edu.cn
*CJ and PZ contributed equally to this work.
Additional Supporting Information may be found in the online version of this article.

Journal of Bone and Mineral Research, Vol. 32, No. 3, March 2017, pp 508–521
DOI: 10.1002/jbmr.3009

osteogenic differentiation efficiently. Mechanistically, *SLC7A11* knockdown and SAS treatment increased BMP2/4 expression. Notably, SAS treatment alleviated bone loss in ovariectomized (OVX) mice effectively. These encouraging data suggested that SAS is a promising therapeutic agent to prevent osteoporosis via inhibition of SLC7A11.

Materials and Methods

Isolation and culture of MSCs

Primary human adipose-derived stem cells and bone marrow MSCs were purchased from ScienCell Research Laboratories (Carlsbad, CA, USA). Cells from three donors were used for the in vitro and in vivo experiments. All cell-based in vitro experiments were repeated in twice. To induce osteogenic differentiation, MSCs were cultured in osteogenic media containing 100 nM dexamethasone (Sigma-Aldrich, St. Louis, MO, USA), 0.2 mM ascorbic acid (Sigma-Aldrich), and 10 mM β-glycerophosphate (Sigma-Aldrich). To induce adipogenic differentiation, MSCs were cultured in adipogenic medium containing 10 μM insulin (Sigma-Aldrich), 100 nM dexamethasone (Sigma-Aldrich), 0.5 mM 3-isobutyl-1-methylxanthine (Sigma-Aldrich), and 200 μM indomethacin (Sigma-Aldrich).

Mouse bone marrow mesenchymal stem cells (mMSCs) samples were collected from SHAM and OVX mice by flushing the femurs and tibias with complete medium containing Dulbecco's Modified Eagle's Medium (DMEM) (Invitrogen, Carlsbad, CA, USA), 10% fetal calf serum (FBS) (PAA Laboratories GmbH, Linz, Austria), and penicillin/streptomycin (Invitrogen). The bone marrow suspension was concentrated, washed twice in DMEM and then cultured at 37°C in a 5% CO_2 atmosphere. Cells were collected after 2 weeks when the mMSCs had expanded.

Viral infection

Viral packaging and infection were performed as described.[24]

The shRNA target sequences were as follows:

scrambled non-target shRNA (NC), TTCTCCGAACGTGTCA CGTTTC;
*SLC7A11*sh#1, GCAGCTACTGCTGTGATATCC; and
*SLC7A11*sh#2, GCAGCTAATTAAAGGTCAAAC.

Alkaline phosphatase staining

MSCs were seeded in six-well plates and cultured for 7 days under proliferation media (PM) or osteogenic media (OM). The cells were then rinsed three times with phosphate-buffered saline (PBS), fixed in 4% paraformaldehyde at room temperature (RT) for 15 min and washed three more times with PBS. For staining, an alkaline phosphatase (ALP) substrate solution (CWBIO, Beijing, China) was added to the fixed cells for 15 min at room temperature. Cells were then washed three times with distilled water, and images were scanned.

Quantification of ALP activity

The cells were washed three times with PBS and lysed with 1% TritonX-100 (Sigma-Aldrich) for 10 min on ice. The cells were then collected using a cell scraper and centrifuged at 13362 *g* for 30 min at 4°C. The protein concentration of supernatants was measured using a BCA protein assay kit (Prod#23225; Pierce Thermo Scientific, Waltham, MA, USA), according to the manufacturer's instructions. ALP activity was assayed using an ALP assay kit (A059-2; Nanjing Jiancheng Bioengineering Institute, Nanjing, China) and calculated after normalization to the total protein content.

Alizarin red S staining and quantification

Cells were washed three times with distilled water, fixed with 4% paraformaldehyde for 10 min at room temperature, and washed three times again with distilled water. The cells were then stained with 2% Alizarin red S staining solution (pH 4.2; Sigma Aldrich) for 30 min at room temperature. Images were recorded with a scanner. For quantification of mineralization, the staining was solubilized with 100 mM cetylpyridinium chloride (Sigma-Aldrich) for 1 hour and measured spectrophotometrically at 562 nm.

Oil red O staining

The cells were washed with PBS three times and fixed in 10% formalin for 20 min. The cells were then rinsed with 60% isopropanol and stained for 60 min at room temperature with filtered Oil red O (0.3%; Sigma-Aldrich). Finally, the cells were washed with distilled water, examined under a microscope, and photographed.

Determination of cellular glutathione

Glutathione (GSH) was measured using a GSH Assay kit (Nanjing Jiancheng Bioengineering Institute) according to the manufacturer's instructions. Briefly, cells were collected, sonicated, mixed with Reagent 1, and then centrifuged at 1485 *g* for 10 min. The supernatant was used as the substrate in a chromogenic reaction and the reaction was measured spectrophotometrically at 420 nm.

Real-time qPCR

Total RNA was extracted with TRIzol reagent (Invitrogen), and the concentration and purity of the total RNA were determined using a Nano Drop 8000 (Pierce Thermo Scientific). RNA with optical density (OD) 260/280 nm ratios between 1.8 and 2.0 were used for cDNA synthesis. Reverse transcription was conducted with a PrimeScript RT Reagent Kit (Takara, Tokyo, Japan; #RR037A). qPCR was performed with SYBR Green Master Mix (Roche Applied Science, Mannheim, Germany) in combination with a 7500 Real-Time PCR Detection System (Applied Biosystems, Foster City, CA, USA) using GAPDH for normalization. *SLC7A11*, (F) TTCACAACCATTAGTGCCGAGG, (R) GCATTATCATTGTCAAAGGGTG; *ALP*, (F) ATGGGATGGGTGTCTCCACA, (R) CCACGAAGGGGAACTTGTC; *RUNX2*, (F) CCGCCTCAGTGATTTAGGGC, (R) GGGTCTGTAATCTGACTCTGTCC; osteocalcin (*OCN*), (F) CACTCCTCGCCCTATTGGC, (R) CCCTCCTGCTTGGACACAAAG; *OSX*, (F) AGCAGCAGTAGCAGAAGCA, (R) CAGCAGTCCCATAGGCATC; human *GAPDH*, (F) GGTCACCAGGGCTGCTTTTA, (R) GGTCGACCTTTAGGAGACCGCA; *BMP2*, (F) CCTTGCGCCAGG TCCTTTGA, (R) GGTCGACCTTTAGGAGACCGCA; *BMP4*, (F) CGTCCAAGCTATCTCGAGCCTG, (R) GAATGGCTCCATAGGTCCC TGC; *BMPR1A*, (F) TTCCCTGGGGTCCGGACTTA, (R) ACGACTCCTCCAAGATGTGGC; *BMPR1B*, (F) AGCCTGCCATAAGTGAGAAGCAAA, (R) GGTGGTGGCATTTACAACGCA. Mouse *Gapdh*, (F) ACAGCAAC TCCCACTCTTCCAC, (R) AGTTGGGATAGGGCCTCTCTTG; Mouse *Slc7a11*, (F) ATCTCCCCCAAGGGCATACT, (R) GCATAGGACAGGG CTCCAAA.

Western blotting

MSCs were washed three times with cold PBS, and lysed in radioimmunoprecipitation assay (RIPA) buffer supplemented with protease inhibitor cocktail (Roche). After centrifugation of the cell lysate at 13362 *g* at 4°C for 30 min, supernatants were transferred to new tubes, and their protein concentrations were determined using the BCA protein assay (Thermo Scientific). Total protein (25 μg) of each sample was subjected to 10% SDS-PAGE. After electrophoresis, proteins were transferred to a polyvinylidene fluoride membrane (Millipore, Billerica, MA, USA) and the membrane was blocked with 5% nonfat milk in Tris-buffered saline (TBS) and then incubated with anti-SLC7A11 (Abcam, Cambridge, UK), anti-OCN (Abcam), anti-BMP2 (Abcam), anti-BMP4 (Abcam), anti-p-Smad1/5/8 (Cell Signaling Technology, Beverly, MA, USA), anti-Smad1 (Abcam), anti-p-eIF2α (Cell Signaling Technology), anti-eIF2α (Cell Signaling Technology), or anti-GAPDH (Abcam) in TBS at 4°C overnight. The membrane was washed with TBS-Tween 20 (TBST) buffer and subsequently incubated with goat anti-rabbit IgG (Abcam) and then washed with TBST buffer again to remove unbound antibody. The bands were visualized using an ECL Western blot kit (CW0049C; CWBIO). The intensities of the bands were quantified using ImageJ software (NIH, Bethesda, MD, USA; https://imagej.nih.gov/ij/).

Heterotopic bone formation assay in vivo

The human MSCs were collected and incubated with hydroxyapatite/tricalcium phosphate (HA/TCP) carrier (Geistlich; GEWO GmbH, Baden-Baden, Germany) scaffolds for 1 hour at 37°C, followed by centrifugation at 150*g* for 5 min, and then implanted subcutaneously on the backs of 6-week-old BALB/C homozygous nude (nu/nu) mice (five mice per group). Sample preparation and histomorphometric analysis were performed as described.[25] Briefly, the bone constructs were fixed in 4% paraformaldehyde and then decalcified for 10 days in 10% EDTA (pH 7.4). After decalcification, the specimens were dehydrated and subsequently embedded in paraffin. Sections (5-μm-thick) were stained with hematoxylin and eosin (H&E) and Masson's trichrome stain. To quantify bone-like tissue, 10 images of each sample were taken randomly (Olympus, Tokyo, Japan) and SPOT 4.0 software (Diagnostic Instruments, Sterling Heights, MI, USA) was used to measure the area of new bone formation versus total area. All animal experiments in this study were carried out with the approval of Peking University Biomedical Ethics Committee Experimental Animal Ethics Branch.

SAS treatment on transplants in vivo

Forty-five 6-week-old BALB/C homozygous nude mice (Vital Co, Beijing, China) were divided into three groups (15 mice per group) as follows: (1) cells and HA/TCP carriers without SAS; (2) cells treated with 0.1 mM SAS for 1 week and then seeded on HA/TCP carriers; and (3) cells incubated with SAS-infused HA/TCP carriers. The cells were then implanted subcutaneously into the dorsal side of the mice. Eight weeks later, the samples were obtained, decalcified, and stained using immunohistochemistry (IHC) and tartrate-resistant acid phosphatase (TRAP) staining.

Micro-computed tomography analysis of bones from mice

BALB/C mice were obtained from Vital Co., and maintained in a pathogen-free facility on a 12-hour light/dark cycle with water and food provided *ad libitum*. Three-month-old mice were sham-operated (SHAM) or OVX. Subsequently, the OVX mice presented osteoporosis, as described.[26] After 2 months of ovariectomy surgery, mice were euthanized for the related assays.

The proximal femur and tibia were thoroughly dissected free of soft tissue and fixed with 4% paraformaldehyde for 24 hours and subsequently washed with 10% sucrose solution. Twelve hours later, micro-CT (μCT) images were scanned at a resolution of 9.088 μm, with tube voltage of 60 kV, tube current of 220 μA, and exposure time of 800 ms in each of the 360 rotational steps. A typical examination consisted of a scout view, selection of the examination volume, automatic positioning, measurement, offline reconstruction, and evaluation. Two-dimensional (2D) images were used to generate three-dimensional (3D) reconstructions using multimodal 3D visualization software (Inveon Research Workplace; Siemens, Munich, Germany) supplied by the μCT system.

Parameters were calculated using an Inveon Research Workplace (Siemens) as follows: bone volume/total volume (BV/TV), trabecular thickness (Tb.Th), trabecular number (Tb.N), and trabecular separation (Tb.Sp) in the trabecular region (0.5 to 1 mm distal to the proximal epiphysis) according to guidelines set by the American Society for Bone and Mineral Research (ASBMR).[27]

Implantation of the Alzet mini-osmotic pump

Female BALB/C mice (3 months old, weighing 25 to 30 g) were purchased from Vital Co., and kept under specific pathogen-free (SPF) conditions. Animals were randomized into four groups of 20 animals each. Group one was sham operated (SHAM), group two was SHAM and treated with SAS (SHAM+SAS), group three was ovariectomized (OVX), and group four was OVX and treated with SAS (OVX+SAS). Animals were anesthetized with 1% sodium pentobarbital via intraperitoneal injection. Then, for OVX mice, both ovaries were removed after performing a low midline incision on the abdominal wall. Sham surgery was done by simply opening the abdomen without performing ovariectomy. One month after surgery, all animals were implanted with an Alzet mini-pump (Alzet, Cupertino, CA, USA) under the skin of the back. The Alzet pumps used were model 2004 pumps, which could deliver 0.25 μL/hour, or a total of 200 μL over 4 weeks. Alzet pumps were filled according to the manufacturer's instructions and put into physiological saline in the SHAM and OVX groups. The other two groups were implanted with Alzet pumps containing a 80-mg dose of SAS for 1 month of continuous delivery. Ten mice from each group were euthanized at weeks 4 and 8, respectively, after ALZET operation. Femurs were harvested, cleaned free of soft tissues and fixed in 4% paraformaldehyde for 24 hours. The femurs were scanned by μCT, followed by H&E staining. Samples were prepared as described.[24]

Statistical analysis

All statistical analyses were performed using the GraphPad scientific software for Windows (San Diego, CA, USA). Comparisons between two groups were analyzed by independent two-tailed Student's *t* tests, and comparisons between more than two groups were analyzed by one-way ANOVA, followed by a Tukey's post hoc test. Data were expressed as the mean ± standard deviation (SD) of three to 10 experiments per group. Values of $p < 0.05$ were considered statistically significant.

Results

Endogenous expression of SLC7A11 is significantly downregulated in MSCs undergoing osteogenic differentiation

First, we analyzed the endogenous expression profile of SLC7A11 in MSCs after osteogenic differentiation. Interestingly, real-time qPCR (RT-qPCR) showed that decreased expression of *SLC7A11* was accompanied by upregulation of osteogenic markers *RUNX2*, *OCN*, and *ALP* (Fig. 1*A–D*). Western blotting showed a similar pattern at the protein level, (Fig. 1*E*, *F*). In addition, immunofluorescence staining revealed that the percentage of SLC7A11-positive MSCs was lower in osteogenic media than in proliferation media (Supporting Fig. S1). Taken together, these results demonstrated that SLC7A11 expression was inversely correlated with the expression of osteogenic markers when MSCs differentiate along the osteogenic lineage.

Knockdown of SLC7A11 significantly enhanced the osteogenic differentiation potential of MSCs in vitro

To investigate the impact of SLC7A11 on the osteogenic ability of MSCs, we first generated a stable cell line with lentiviruses expressing *SLC7A11* shRNA. To rule out off-target effects, two shRNA sequences against SLC7A11 were designed. Fluorescent staining and Western blotting confirmed the efficiency of knockdown (Supporting Fig. S2A, Fig. 2*A*). After culturing MSCs in osteogenic media for 7 days, the ALP activity of differentiating MSCs was significantly increased by *SLC7A11* knockdown (Fig. 2*B*, *C*). Moreover, extracellular matrix mineralization, as shown by Alizarin red S staining and quantification at 2 weeks after osteogenic induction, was also increased dramatically in *SLC7A11* shRNA-treated cells compared with control shRNA-treated cells (Fig. 2*D*, *E*). To further confirm that SLC7A11 depletion promoted osteogenic differentiation of MSCs, we assessed the mRNA expression of several osteogenic markers after induction. As shown in Fig. 2*F–H* and Supporting Fig. S2B, *SLC7A11* knockdown significantly promoted the expressions of *RUNX2*, *OCN*, *ALP*, and *IBSP*. Collectively, these results indicated that SLC7A11 is a negative regulator of osteogenic differentiation in vitro. To further explore the potential role of SLC7A11 in regulating adipogenic differentiation of MSCs, *SLC7A11* sh MSCs and control cells were grown in adipogenic media. After 3 weeks of culture, we performed Oil-Red-O staining to detect the lipid droplets. As shown in Supporting Fig. S2C, we observed decreased adipogenesis in *SLC7A11* sh MSCs compared with control cells. In addition, the depletion of *SLC7A11* inhibited the mRNA level of the master adipogenic transcription factor *PPAR-γ*, as shown in Supporting Fig. S2D.

SLC7A11 knockdown accelerated the osteogenic differentiation of MSCs in vivo

H&E staining showed that MSCs/*SLC7A11*sh#1 and MSCs/*SLC7A11*sh#2 cells formed much more bone tissues than MSCs/NC cells (Fig. 3*A*). Quantitative measurement of mineralized tissue areas revealed an increase of more than 50% in bone formation by MSCs/*SLC7A11*sh#1 and MSCs/*SLC7A11*sh#2 cells compared with MSCs/NC cells (Supporting Fig. S3A). Consistently, Masson's trichrome staining also showed that bone-like tissues were markedly increased for hybrids containing MSCs/*SLC7A11*sh#1 and MSCs/*SLC7A11*sh#2 compared with control cells (Fig. 3*B*). Because SLC7A11 is pivotal for the synthesis of GSH, we next investigated intracellular GSH levels during osteogenesis. The results showed that the levels of intracellular GSH decreased during osteogenic differentiation in a time-dependent manner (Supporting Fig. S3B). Moreover, *SLC7A11* knockdown and SAS treatment also reduced the levels of GSH (Supporting Fig. S3C, D). Given that cystine is a precursor for the synthesis of GSH, we examined the role of cystine on osteogenic differentiation. We used DMEM with 100% cystine, 30% cystine, and 10% cystine to prepare proliferation medium and osteogenic medium, respectively. ALP staining and activity showed that osteogenic differentiation was enhanced by cystine reduction, as shown in Supporting Fig. S3E, F. Next, we treated cells with cystine deprivation for 24 hours, and performed GSH assay, the results showed that GSH levels decreased after cystine deprivation (Supporting Fig. S4A). In addition, we discovered that cystine deprivation induced *BMP2* and *BMP4* expression in a time-dependent manner, as measured by RT-qPCR (Supporting Fig. S4B, C). We also found cystine reduction (DMEM with 100%, 70%, 50%, 30%, 10%, and 0% cystine, respectively) increased *BMP2* and *BMP4* expression in a dose-dependent manner (Supporting Fig. S4D, E). Western blotting showed that cystine deprivation increased the protein expression of BMP2, BMP4, and p-Smad1/5/8 (Supporting Fig. S4F, G). These data indicated that GSH and cystine play critical roles in SLC7A11-regulated osteogenesis.

The SLC7A11 inhibitor SAS promoted osteogenic differentiation effectively both in vitro and in vivo

To further confirm our results, we measured the osteogenic differentiation potential of MSCs in the presence of SAS, a potent and relatively selective competitive inhibitor of SLC7A11. As shown in Supporting Fig. S5A–D, SAS treatment significantly promoted the expressions of osteogenesis-associated genes *RUNX2*, *ALP*, *OCN*, and *OSX* in a dose-dependent manner when added at concentrations 0.05 mM and 0.1 mM. To further clarify the potential role of SAS in osteogenic differentiation, MSCs with or without SAS treatment were cultured in osteogenic media for 7 days; ALP activity found to be increased significantly in cells treated with SAS (Fig. 4*A*, *B*). Moreover, Alizarin Red S staining and quantification showed that extracellular matrix mineralization was also increased by SAS treatment at 2 weeks after osteogenic induction (Fig. 4*C*, *D*). Next, we examined the role of SAS in vivo. Six-week-old BALB/C homozygous nude mice were divided into three groups (15 mice per group), and then implanted subcutaneously with either (1) cells and HA/TCP carriers without SAS, (2) cells treated with 0.1 mM SAS for 1 week, or (3) cells incubated with SAS-infused HA/TCP carriers. As shown in (Fig. 4*E*, *F*), SAS treatment promoted bone formation in vivo significantly. It was reported that the cystine/glutamate antiporter could modulate osteoclastogenesis.[28] We then performed TRAP staining to examine the osteoclastogenesis under SAS treatment. Supporting Fig. S5E shows that SAS treatment reduce the number of osteoclasts, which correlated with decreased SLC7A11 activity (Supporting Fig. S5F). To determine whether SAS affects adipocyte differentiation, adipogenic medium was supplemented with different concentrations of SAS. As shown in Supporting Fig. S6A, SAS treatment significantly inhibited adipogenesis associated genes *PPAR-γ* expression in a dose-dependent manner. Oil red O staining further validated these observations (Supporting Fig. S6B).

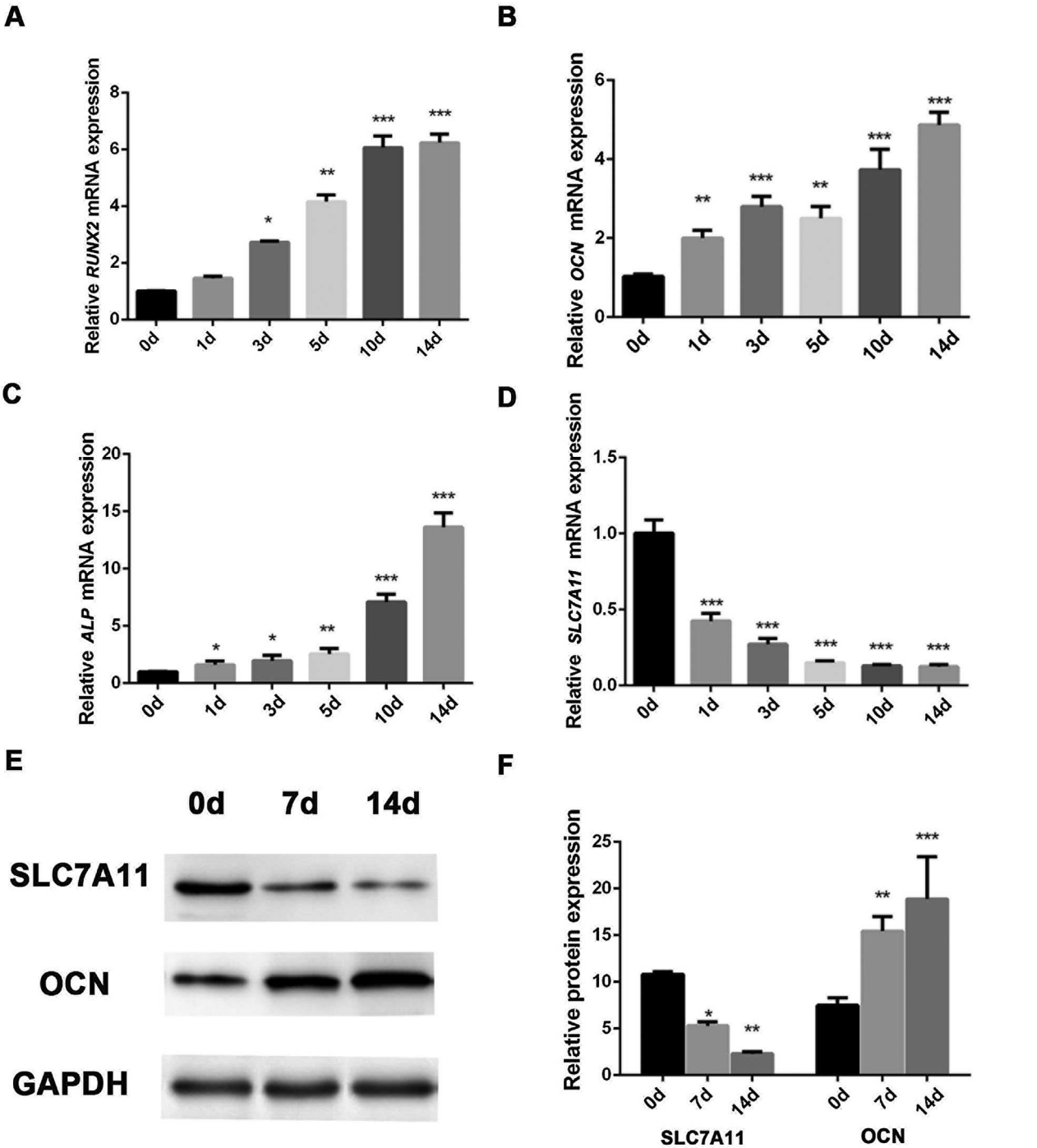

Fig. 1. Endogenous SLC7A11 is downregulated during osteogenic differentiation of MSCs. (*A–C*) RT-qPCR analysis performed on MSCs undergoing to osteogenesis revealed a significant upregulation of *RUNX2* (*A*), *OCN* (*B*), and *ALP* (*C*) gene expression. Conversely, *SLC7A11* gene expression was significantly downregulated upon osteogenic differentiation (*D*). (*E*) Western blotting analysis of SLC7A11 proteins performed using a specific anti-SLC7A11 antibody confirmed the observed gene expression patterns. (*F*) Quantification of the SLC7A11 expression level obtained in *E* using Image J. All data are shown as the mean ± SD, $n = 3$. $^{*}p < 0.05$, $^{**}p < 0.01$, and $^{***}p < 0.001$, compared with day 0 day. PM = proliferation media; OM = osteogenic media.

Knockdown of *SLC7A11* or SAS treatment increased the BMP2/4 expression

Next, to determine the mechanisms underlying the regulation of osteogenic differentiation by SLC7A11, stable *SLC7A11* knockdown cells were subjected to mRNA determination and protein expression analysis for several key regulators of osteogenesis. Surprisingly, a significant increase of *BMP2* and *BMP4* mRNA expression was detected in *SLC7A11* knockdown cells (Fig. 5*A*). Furthermore, Western blotting and quantification of the electrophoresis bands showed that downregulation of SLC7A11 could promote BMP2/4 expression at the protein level

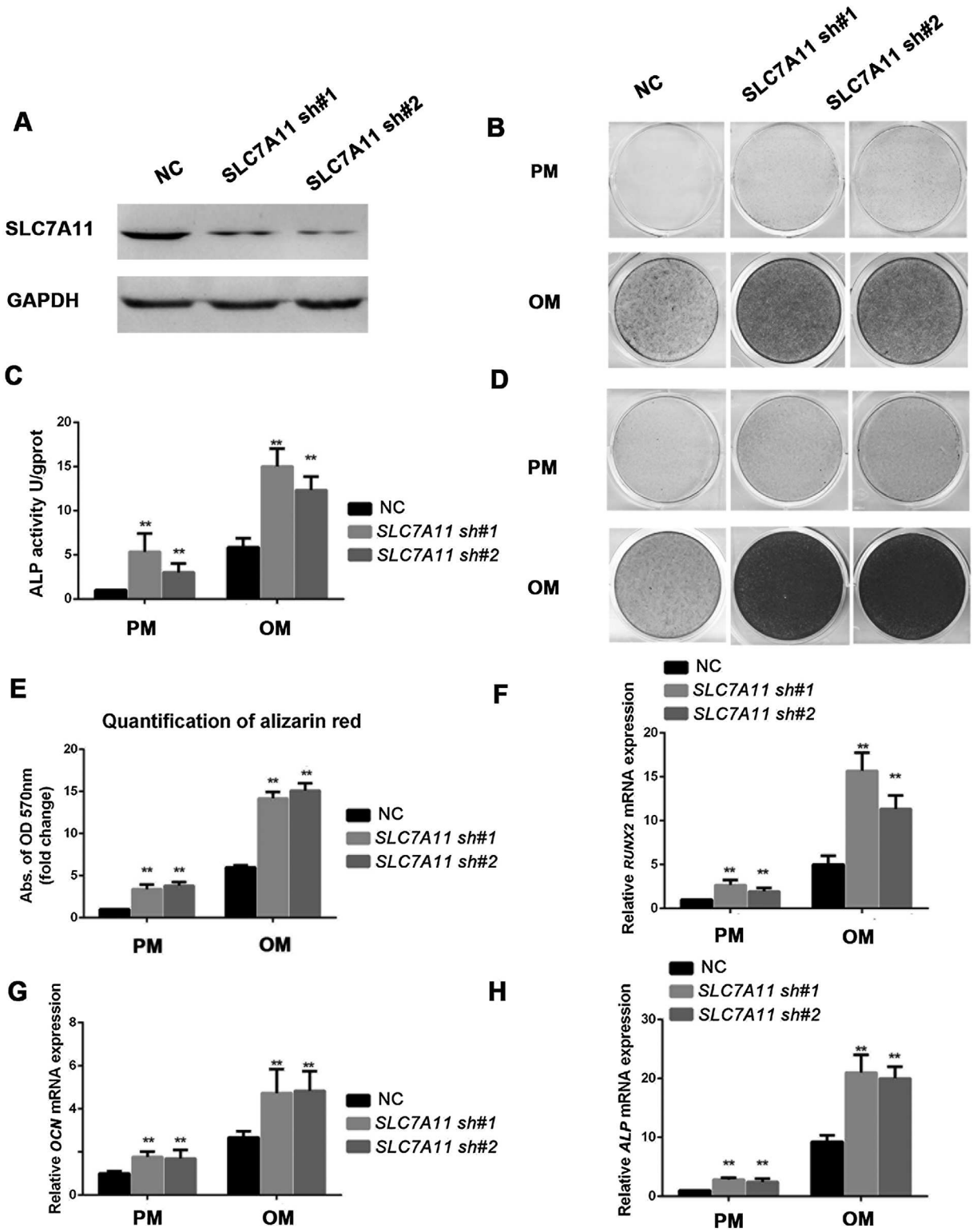

Fig. 2. Knockdown of *SLC7A11* enhances osteogenic differentiation of MSCs in vitro. (*A*) Knockdown of *SLC7A11* expression was validated by Western blotting. (*B*, *C*) *SLC7A11* knockdown increased ALP activity in MSCs. Control or *SLC7A11* knockdown MSCs were treated with PM or OM for 7 days for ALP staining (*B*), and cellular extracts were prepared to quantify ALP activity (*C*). (*D*, *E*) Knockdown of *SLC7A11* accelerated mineralization of MSCs. Cells with or without *SLC7A11* knockdown were treated with PM or OM for 14 days, and then calcium deposition was observed using Alizarin Red S staining (*D*) and quantified (*E*). Knockdown of *SLC7A11* promoted the expression of *RUNX2* (*F*), *OCN* (*G*), and *ALP* (*H*) in MSCs, as determined by RT-qPCR. All data are shown as the mean ± SD, $n = 3$. $^{**}p < 0.01$, compared with NC. PM = proliferation media; OM = osteogenic media.

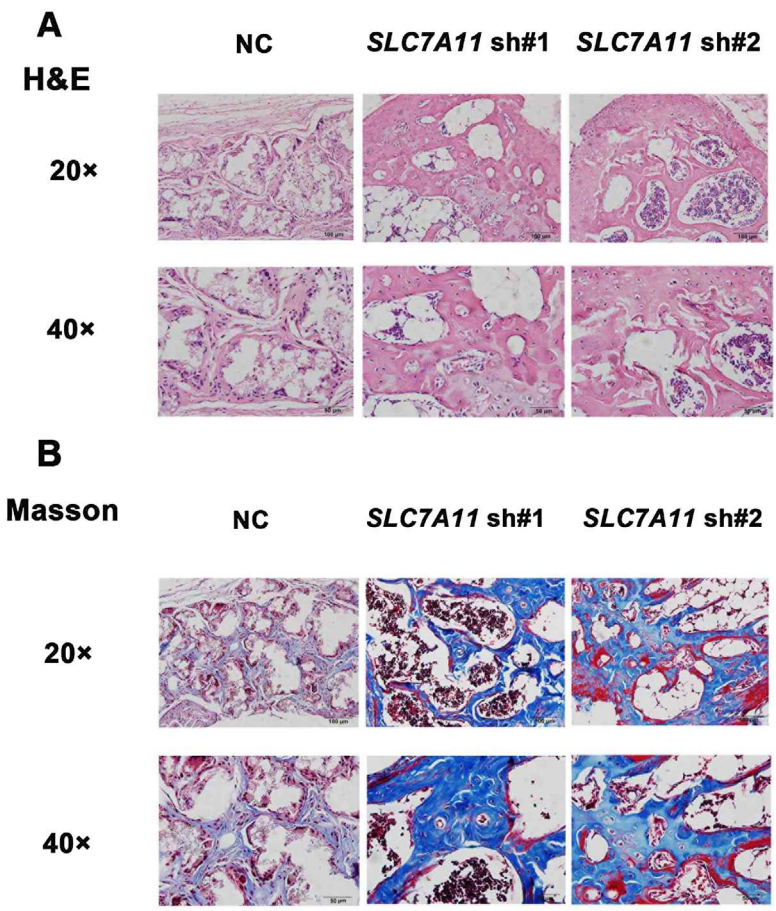

Fig. 3. Knockdown of *SLC7A11* significantly induced MSCs-mediated bone formation in vivo. (*A*) H&E staining from implanted MSCs-scaffold hybrids, as indicated. (*B*) Masson's trichrome staining of histological sections from implanted MSCs-scaffold hybrids, as indicated.

(Fig. 5*B*, *C*). To compare the relative effects of knockdown of *SLC7A11* and SAS on *BMP2/4* expression directly, we detected *BMP2/4* expression in the presence or absence of SAS. As shown in Supporting Fig. S6C–E, 0.1 mM SAS treatment enhanced both mRNA and protein levels of BMP2/4 significantly. To explore the mechanism by which the BMP signaling pathway is involved in the SLC7A11-mediated differentiation of osteoblasts, we studied the downstream signaling molecules p-Smad1/5/8 in *SLC7A11* knockdown and SAS-treated cells: the protein expression levels of p-Smad1/5/8 were increased significantly in *SLC7A11* knockdown cells (Fig. 5*B*, *C*; Supporting Fig. S6D, E). To further verify that the BMP signaling is involved in SLC7A11-regulated osteogenesis, we established *SLC7A11* and *SMAD1* double knockdown cells. Western blotting experiments were employed to detect the knockdown efficiency (Supporting Fig. S6F, G). As shown in Fig. 5*D*, *E*, when cells were treated with osteogenic media, the increase in osteogenic differentiation conferred by *SLC7A11* knockdown was effectively reversed in the *SLC7A11* and *SMAD1* double knockdown cells, as indicated by ALP staining and quantification. Moreover, Alizarin Red S staining and quantification showed that extracellular matrix mineralization was also decreased in *SLC7A11* and *SMAD1* double knockdown cells compared with *SLC7A11* knockdown cells after osteogenic induction (Fig. 5*F*, *G*). In addition, compared with the control cells, knockdown of *SLC7A11* and *SMAD1* resulted in decreased mRNA expressions of *RUNX2* and *ALP* (Supporting Fig. S6H, I). Next, we detected the effect of the BMP antagonist Noggin in *SLC7A11* knockdown and SAS-treated cells. As shown in Fig. 5*H–I*, Supporting Fig. S7A–F, and Supporting Fig. S8A–D, Noggin treatment blocked the increased osteogenic differentiation caused by *SLC7A11* knockdown or SAS treatment effectively.

Previous experimental evidence suggested that amino acid limitation activated general control non-derepressible-2 (GCN2) protein kinase, which subsequently phosphorylated the translation initiation factor eIF2α.[29] Hence we tested the level of phosphorylation of eIF2α in *SLC7A11* knockdown cells, and found that *SLC7A11* knockdown increased the level of phosphorylated eIF2α (Supporting Fig. S8E, F).

SLC7A11 expression was increased in osteoporotic mice

MSCs in bone marrow can differentiate into either osteoblasts or adipocytes, and there is an inverse relationship between osteogenesis and adipogenesis in MSC differentiation.[30–32] Our results suggested that the status of SLC7A11 may be a critical factor that determines MSC fate in bone marrow. To test this hypothesis, we established an OVX mouse model. μCT and H&E staining showed that the trabecular bone was significantly reduced in OVX mice compared with SHAM mice (Fig. 6*A–D*, Supporting Fig. S8G–H). Next, we isolated MSCs from both SHAM and OVX mice. RT-qPCR revealed that the expression of

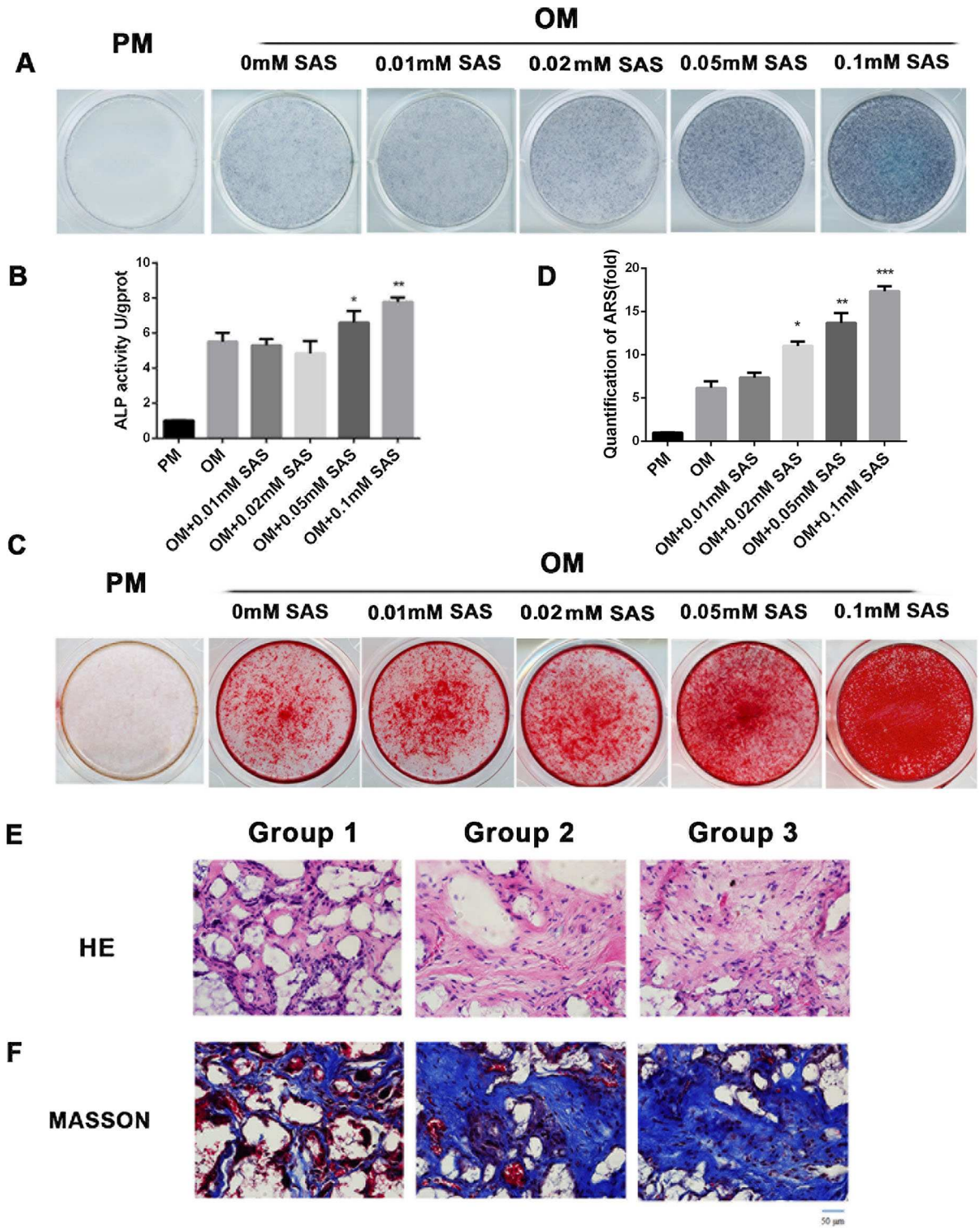

Fig. 4. SAS promoted osteogenic differentiation of MSCs both in vitro and in vivo. (*A*, *B*) MSCs with or without SAS treatment were treated with PM or OM for ALP staining (*A*), and cellular extracts were prepared to quantify ALP activity (*B*). (*C*, *D*) SAS at 0.05 mM and 0.1 mM accelerates mineralization of MSCs. Cells in the presence or absence of SAS treatment were treated with PM or OM for 14 days, and then calcium deposition was observed using Alizarin Red S staining (*C*) and quantified (*D*). (*E*, *F*) H&E staining (*E*), Masson's trichrome staining (*F*) in group 1 (cells and HA/TCP carriers without SAS), group 2 (cells treated with 0.1 mM SAS for 1 week and then seeded on HA/TCP carriers), and group 3 (cells incubated with SAS infused HA/TCP carriers). Scale bar = 50 μm. All data are shown as the mean ± SD, $n = 3$. $^{*}p < 0.05$, $^{**}p < 0.01$, and $^{***}p < 0.01$, compared with PM. PM = proliferation media; OM = osteogenic media; HA/TCP = hydroxyapatite/tricalcium phosphate.

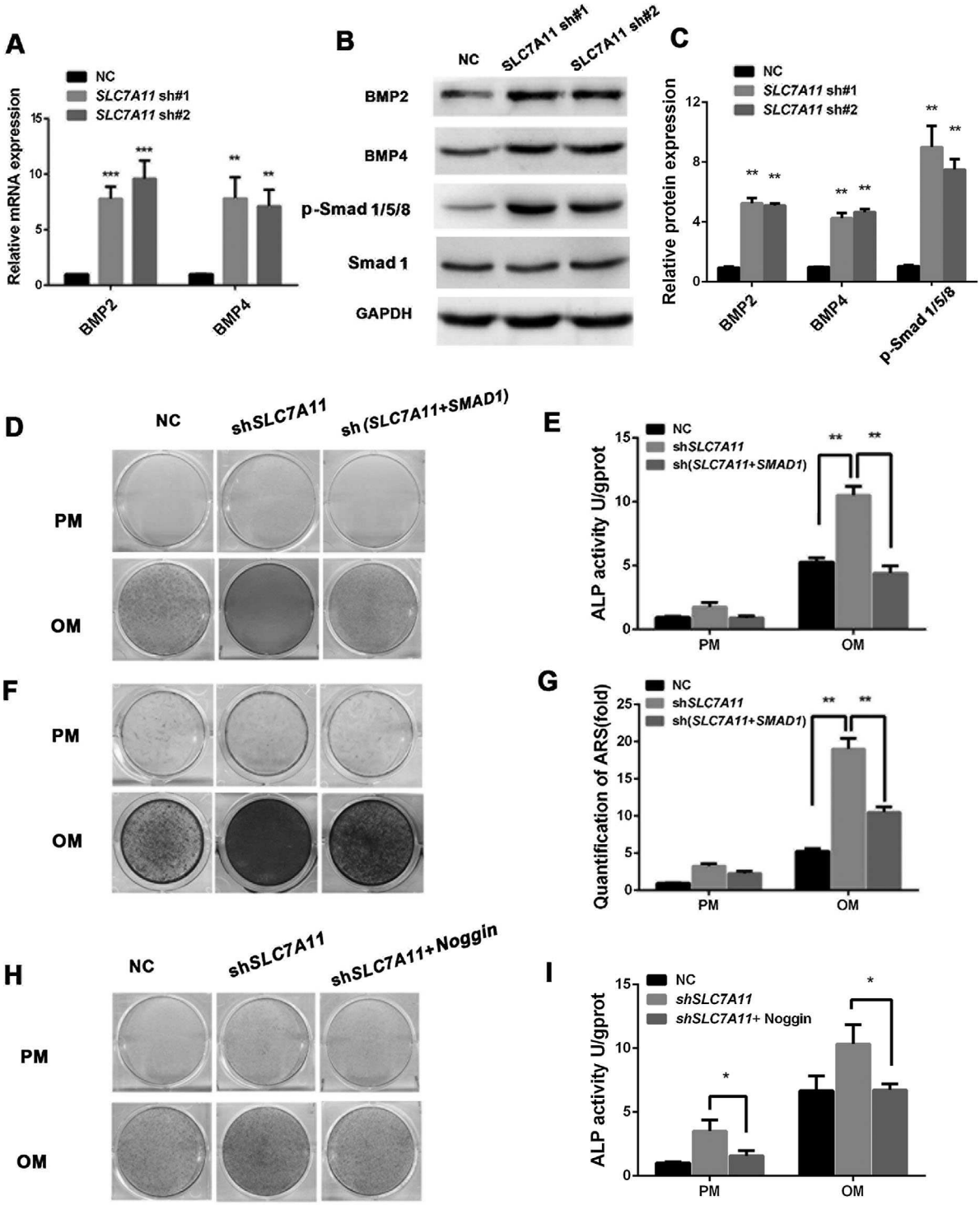

Fig. 5. *SLC7A11* knockdown enhanced osteogenesis of MSCs through BMP-Smads signaling. (*A*) RT-qPCR analysis shows the significant induction of *BMP2* and *BMP4* in *SLC7A11* knockdown cells. (*B*) Western blotting analysis showing increased expression of BMP2, BMP4, and p-Smad1/5/8 in *SLC7A11* sh MSCs. (*C*) Quantification of BMP2, BMP4, Smad1, and p-Smad1/5/8 expression levels obtained in *B* using Image J, the ratios of both intensities (BMP2/GAPDH, BMP4/GAPDH, p-Smad1/5/8 /Smad1) were calculated. (*D*–*G*) Images of ALP staining (*D*), ARS staining (*F*) in NC, sh*SLC7A11*, and sh(*SLC7A11*+*SMAD1*) groups. Cells were cultured in PM or OM. Histograms show ALP activity (*E*) and quantification of ARS (*G*) staining by spectrophotometry. (*H*, *I*) BMP antagonist Noggin reversed the increase of osteogenesis in *SLC7A11* knockdown cells. Images of ALP staining (*H*), ALP activity (*I*) in NC, sh*SLC7A11*, and sh*SLC7A11* treated with Noggin (500 ng/mL). All data are shown as the mean ± SD, $n = 3$. $^{*}p < 0.05$, $^{**}p < 0.01$, and $^{***}p < 0.001$, compared with NC. ARS = Alizarin Red S; PM = proliferation medium; OM = osteogenic medium.

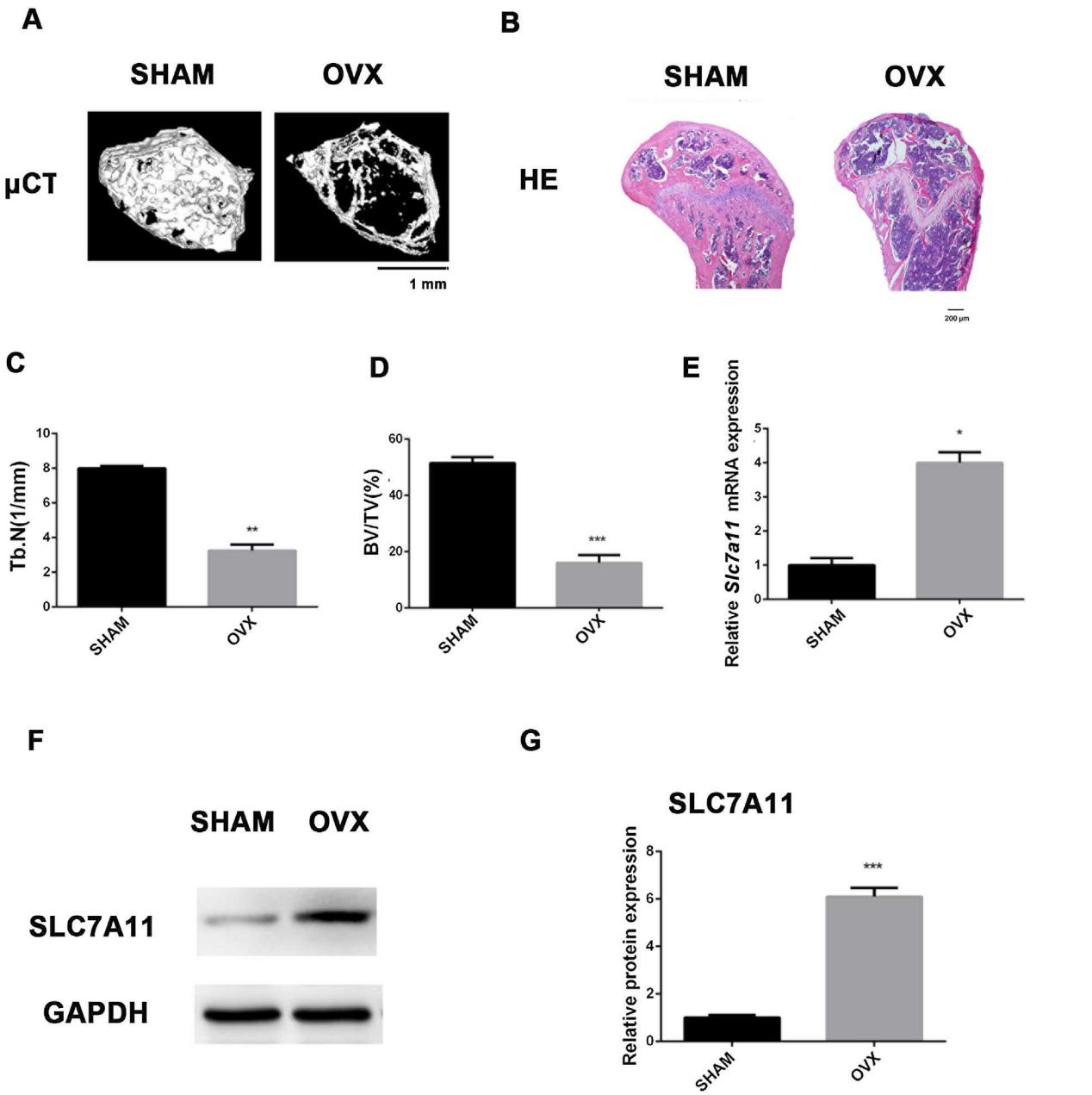

Fig. 6. SLC7A11 in MSCs was significantly increased in the bone marrow of OVX mice. (*A*, *B*) Representative μCT image (*A*) and H&E staining (*B*) of bone loss in OVX mice. Scale bar for μCT in $A = 1$ mm; scale bar H&E in $B = 200$ μm. (*C*) Trabecular number was reduced in OVX mice. (*D*) Bone volume was reduced in OVX mice. (*E*) Expression of *SLC7A11* was induced in bone marrow stem cells from OVX mice compared with SHAM mice, as determined by RT-qPCR. (*F*) Western blotting analysis exhibited increased SLC7A11 expression in bone marrow stem cells of OVX mice. (*G*) Quantitation of SLC7A11 expression level obtained in *F* using Image J. All data are shown as the mean ± SD. $^{*}p < 0.05$, $^{**}p < 0.01$, and $^{***}p < 0.001$ compared with SHAM.

Slc7a11 was increased in MSCs from OVX mice compared with those from SHAM mice (Fig. 6*E*). In addition, Western blotting demonstrated increased SLC7A11 expression in MSCs of OVX mice (Fig. 6*F*, *G*).

SAS treatment attenuates bone loss in OVX mice

To show the clinical significance of our findings, we explored whether the SAS could treat osteoporosis effectively. Eighty 3-month-old female mice were divided into four groups of 20 mice: SHAM, SHAM+SAS, OVX, and OVX+SAS. We first weighed the mice and found that ovariectomy slightly increased the mice's body weight. However, there were no significant differences between mice implanted with SAS or not (as shown in Supporting Fig. S9A). As shown in Fig. 7*A*, μCT and H&E staining showed that there was no significant difference between SHAM mice and SHAM mice with SAS treatment, whereas trabecular bone loss was effectively blocked in OVX mice treated with SAS for 4 weeks. In addition, OVX mice treated with SAS at 8 weeks could also significantly inhibit the bone loss (Fig. 7*B*). Moreover, compared

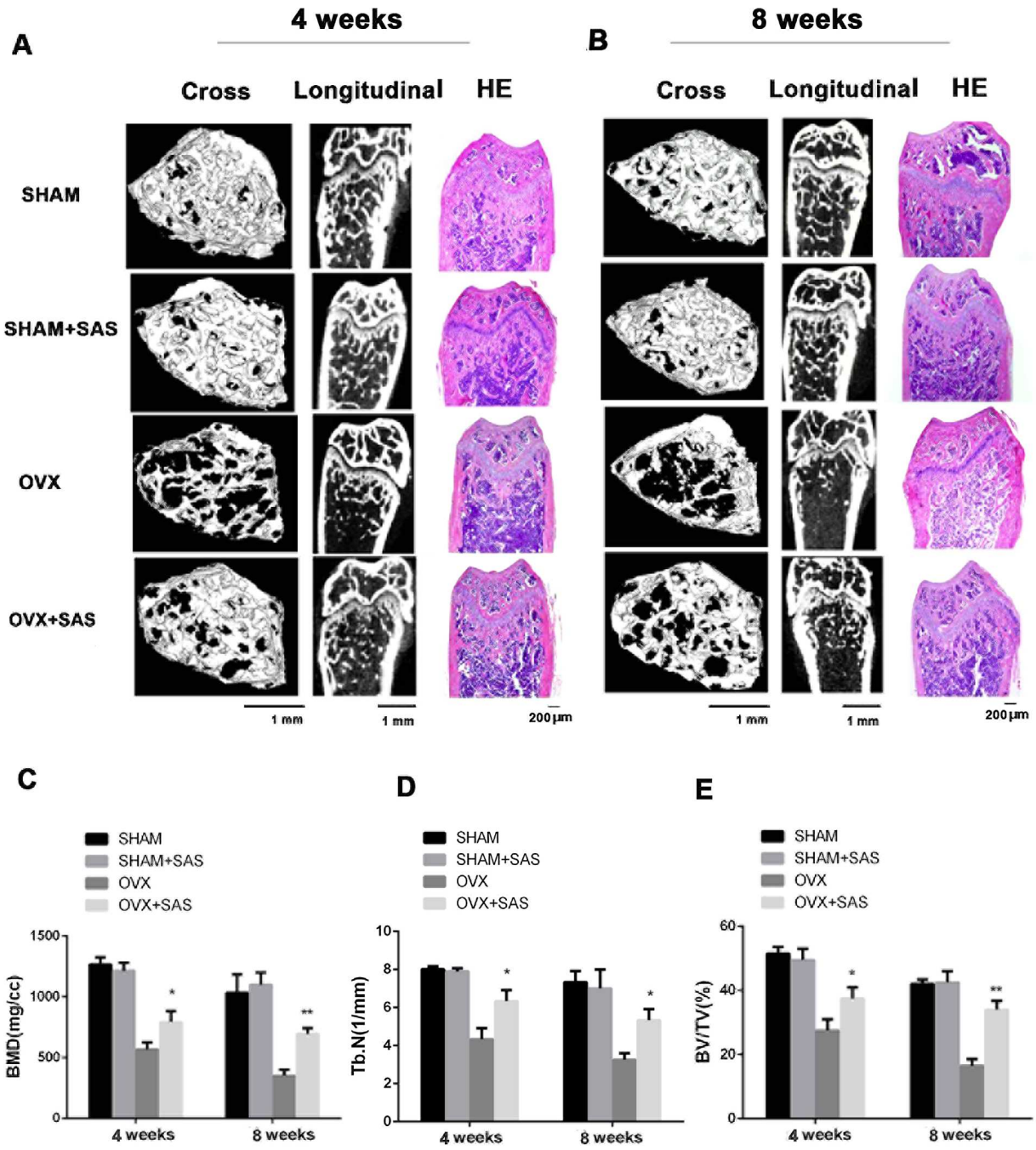

Fig. 7. SAS suppressed bone loss in OVX mice. (*A*, *B*) Representative μCT images in SHAM mice, SHAM mice with SAS treatment, OVX mice, and OVX mice with SAS treatment at 4 weeks (*A*) and 8 weeks (*B*). Scale bar = 1 mm. H&E staining in SHAM mice, SHAM mice with SAS treatment, OVX mice, and OVX mice with SAS treatment at 4 and 8 weeks. Scale bar = 200 μm. (*C*–*E*) OVX mice treated with SAS had different degrees of improvement of BMD (*C*), trabecular number (*D*), and bone volume (*E*) compared with OVX mice. All data are shown as the mean ± SD. $^{*}p < 0.05$, $^{**}p < 0.01$ compared with OVX.

with the SHAM mice, the bone mineral density (BMD) of OVX mice was reduced significantly at the distal femur. However, SAS treatment for the OVX mice partially reversed this bone loss (Fig. 7*C*). Meanwhile, we observed an increased trabecular separation (Supporting Fig. S9B) and a reduction in trabecular number (Fig. 7*D*), bone volume (Fig. 7*E*), and trabecular thickness (Supporting Fig. S9C) in OVX mice, while these parameters were improved to different degrees in the OVX mice treated with SAS. In addition, TRAP staining indicated that the number of osteoclasts increased in OVX group and reduced with SAS treatment (Supporting Fig. 9D, E). To further explore the effect of SAS treatment on mice, we evaluated the protein expression of BMP2 and BMP4 in BMSCs from OVX mice treated with SAS. The results showed that BMP2 and BMP4 decreased in the OVX group, and the SAS-treated group showed significant increase of BMP2 and BMP4 (Supporting Fig. S9F, G).

Discussion

In this study, we found that SLC7A11 expression dramatically decreased during osteogenic differentiation of MSCs. We also observed that SLC7A11 expression inversely correlated with the expression osteogenic markers RUNX2 and OCN. These results suggested that SLC7A11 might prevent MSCs from differentiating toward the osteoblastic lineage. To test this possibility, we downregulated its expression by using a shRNA experimental approach. Upon *SLC7A11* silencing, MSCs acquired an increased ability to differentiate along the osteogenic lineage in vitro. This finding is in agreement with a previous study in which overexpression of *SLC7A11* decreased osteoblastogenesis through downregulation of RUNX2 in MC3T3-E1 cells.[33] However, our present work showed that knockdown of *SLC7A11* significantly accelerated bone formation accelerated bone formation in a bone ossicle model. Most importantly, we discovered that the SLC7A11 inhibitor SAS promoted osteogenic differentiation successfully and suppressed bone loss in OVX mice. Mechanistically, *SLC7A11* knockdown or SAS treatment increased BMP2/4 expression significantly. This study provides valuable clues for the treatment of bone metabolic disease such as osteoporosis.

BMPs play critical roles in the commitment of mesenchymal cells into osteoblast and chondroblast lineages,[34,35] and BMP2/4 enhance osteogenic differentiation of MSCs significantly.[36] Our results showed that knockdown of *SLC7A11* or inhibition of SLC7A11 by SAS treatment could significantly enhance both the mRNA and protein levels of BMP2 and BMP4. This is the first report of a relationship between SLC7A11 and BMPs. The principal biological role of SLC7A11 is the import of cystine, which is an essential precursor for the biosynthesis of the cellular antioxidant GSH.[37] Intracellular GSH plays a critical role in redox regulation through S-glutathionylation of a variety of transcription factors, including nuclear factor-κB (NF-κB), heat shock proteins, and AP-1 components.[38] Mass spectrometry analysis identified a cysteine residue in the conserved catalytic region of deacetylase sirtuin 1 as target for deglutathionylation.[39] There is an elegant study that showed that glutamate suppresses osteoblastogenesis through the cystine/glutamate antiporter in MSCs.[40] In the present study, we detected that the level of intracellular GSH decreased during osteogenic differentiation in a time-dependent manner. We also detected decreased GSH in *SLC7A11* knockdown cells or under SAS treatment. Moreover, we found that cystine reduction promoted osteogenic differentiation of MSCs. In addition, cystine depletion induced decreased GSH levels and induced BMP2 and BMP4 expression in a time-dependent and dose-dependent manner. These results suggested that *SLC7A11* knockdown enhanced the osteogenic differentiation of MSCs by modulating the GSH level. However, the precise molecular mechanism remains unclear. Further experiments will be needed to identify the mechanism of the regulatory control of osteogenesis and BMPs by SLC7A11. It is reasonable to postulate that intracellular GSH would induce the glutathionylation of specific factors that regulate the expression of BMP2/4 in MSCs.

Osteoporosis is associated with severe complications, such as skeletal deformity and increased bone fractures; therefore, efficient treatments for osteoporosis are required urgently.[41] SAS promoted osteogenic differentiation of MSCs; therefore, it was used to treat our osteoporotic OVX mice. To our surprise, SAS treatment could alleviate the bone loss of OVX mice. We also treated SHAM mice with SAS and found SAS did not affect the BMD in normal mice. SAS is a US Food and Drug Administration (FDA)-approved drug that is used widely to treat a number of clinical diseases, for instance, inflammatory bowel diseases (IBD) such as ulcerative colitis (UC) and Crohn's disease (CD).[42,43] Once digested, SAS is cleaved into sulfapyridine and 5-aminosalicylic acid (5-ASA) by colonic bacteria. 5-ASA retains most of the beneficial anti-inflammatory effects of SAS to treat IBD. As an effective second-line drug in rheumatoid arthritis (RA), SAS displays a wide range of anti-inflammatory and immunosuppressive actions, which may account for its mode of action in RA. These include reduced numbers of monocytes, B lymphocytes,[44] serum IgA and IgA-producing cells,[45] and inhibition of leukotriene production.[46] In addition, SAS is effective antitumor drug in a variety of cancers. Two groups used intraperitoneal injection of SAS to inhibit tumor growth successfully. One ascribed the effect of the drug to its inhibition of SLC7A11[47]; the other believed it acted by inhibiting the transcription factor, NF-κB.[48] In the present study, the OVX mice were implanted with Alzet pumps containing SAS for continuous delivery; the SAS was circulated to blood system through subcutaneous tissue, and did not enter the gut to be digested. Note that in clinical treatment, SAS might lead to a series of side effects, including oligospermia, severe immune suppression, gastrointestinal effects, and weight loss. Further clinical investigations are needed to ensure the safe use of SAS in osteoporotic patients. Importantly, the present study indicated that SLC7A11 is a significant target for the treatment of osteoporosis. Additional work will be needed to discover more secure clinical medicines that act on SLC7A11.

It has been previously demonstrated that osteoporosis is related to excessive osteoclast formation and activity.[49] So we also examined the role of SAS on osteoclasts in vivo and found SAS treatment reduced the number of osteoclasts. A lot of studies showed that NF-κB played an essential role for osteoclast differentiation, and blockage of this signaling pathway could inhibit osteoclast formation and function.[50–52] Other studies discovered that SAS inhibited NF-κB expression and activation.[53,54] Considering previous studies, it is possible to postulate that SAS may attenuate osteoporosis of OVX via inhibiting NF-κB activation. However, the function of SAS in vivo is more complex than expected, the precise role and the underlying mechanisms of SAS in regulating osteoblasts and osteoclasts in vivo remain unexplored, further detailed research needs to be done.

In summary, our work shed new light on the role of SAS in osteogenesis and indicated that treatment with SAS is a promising and novel therapeutic approach for osteoporosis. SAS is already FDA-approved for the treatment of other diseases, making a compelling case for further studies of its clinical benefit to treat osteoporosis.

Disclosures

All authors state that they have no conflicts of interest.

Acknowledgments

This study was supported by grants from the National Natural Science Foundation of China (Nos. 81570953, 81500822), the Program for New Century Excellent Talents in University from Ministry of Education (NCET-11-0026), the PKU School of Stomatology for Talented Young Investigators (PKUSS20140109),

and the Construction Program for National Key Clinical Specialty from National Health and Family Planning Commission of China (2011).

Authors' roles: CJ: collection and/or assembly of data, data analysis and interpretation; PZ: conception and design, collection and/or assembly of data, data analysis and interpretation, and manuscript writing; YL: data analysis and interpretation; MZ: data analysis and interpretation; LL: collection and/or assembly of data; XZ: collection and/or assembly of data; HL: collection and/or assembly of data; YZ: conception and design, financial support, manuscript writing, and final approval of manuscript; CJ and PZ contributed equally to this work. All authors read and approved the final version of the manuscript.

References

1. Turner RT, Riggs BL, Spelsberg TC. Skeletal effects of estrogen. Endocr Rev. 1994 Jun;15(3):275–300.
2. Hess R, Pino AM, Ríos S, Fernández M, Rodríguez JP. High affinity leptin receptors are present in human mesenchymal stem cells (MSCs) derived from control and osteoporotic donors. J Cell Biochem. 2005 Jan 1;94(1):50–7.
3. Dalle Carbonare L, Valenti MT, Zanatta M, Donatelli L, Lo Cascio V. Circulating mesenchymal stem cells with abnormal osteogenic differentiation in patients with osteoporosis. Arthritis Rheum. 2009 Nov;60(11):3356–65.
4. Post S, Abdallah BM, Bentzon JF, Kassem M. Demonstration of the presence of independent pre-osteoblastic and pre-adipocytic cell populations in bone marrow-derived mesenchymal stem cells. Bone. 2008 Jul;43(1):32–9.
5. Kang Q, Song WX, Luo Q, et al. A comprehensive analysis of the dual roles of BMPs in regulating adipogenic and osteogenic differentiation of mesenchymal progenitor cells. Stem Cells Dev. 2009 May;18(4):545–59.
6. Dorman LJ, Tucci M, Benghuzzi H, Benghuzzi H. In vitro effects of bmp-2, bmp-7, and bmp-13 on proliferation and differentation of mouse mesenchymal stem cells. Biomed Sci Instrum. 2012;48:81–7.
7. Sato H, Tamba M, Ishii T, Bannai S. Cloning and expression of a plasma membrane cystine/glutamate exchange transporter composed of two distinct proteins. J Biol Chem. 1999 Apr 23;274(17):11455–8.
8. Sato H, Tamba M, Kuriyama-Matsumura K, Okuno S, Bannai S. Molecular cloning and expression of human xCT, the light chain of amino acid transport system xc–. Antioxid Redox Signal. 2000 Winter;2(4):665–71.
9. Kanai Y, Endou H. Heterodimeric amino acid transporters: molecular biology and pathological and pharmacological relevance. Curr Drug Metab. 2001 Dec;2(4):339–54.
10. Kim JY, Kanai Y, Chairoungdua A, et al. Human cystine/glutamate transporter: cDNA cloning and upregulation by oxidative stress in glioma cells. Biochim Biophys Acta. 2001 Jun 6;1512(2):335–44.
11. Chillarón J, Roca R, Valencia A, Zorzano A, Palacín M. Heteromeric amino acid transporters: biochemistry, genetics, and physiology. Am J Physiol Renal Physiol. 2001 Dec;281(6):F995–1018.
12. Verrey F, Closs EI, Wagner CA, Palacin M, Endou H, Kanai Y. CATs and HATs: the SLC7 family of amino acid transporters. Pflugers Arch. 2004 Feb;447(5):532–42.
13. Fernández E, Jiménez-Vidal M, Calvo M, et al. The structural and functional units of heteromeric amino acid transporters. The heavy subunit rBAT dictates oligomerization of the heteromeric amino acid transporters. J Biol Chem. 2006 Sep 8;281(36):26552–61.
14. Chintala S, Li W, Lamoreux ML, et al. Slc7a11 gene controls production of pheomelanin pigment and proliferation of cultured cells. Proc Natl Acad Sci U S A. 2005 Aug 2;102(31):10964–9.
15. Sato H, Shiiya A, Kimata M, et al. Redox imbalance in cystine/glutamate transporter-deficient mice. J Biol Chem. 2005 Nov 11;280(45):37423–9.
16. De Bundel D, Schallier A, Loyens E, et al. Loss of system x(c)– does not induce oxidative stress but decreases extracellular glutamate in hippocampus and influences spatial working memory and limbic seizure susceptibility. J Neurosci. 2011 Apr 13;31(15):5792–803.
17. Lo M, Ling V, Wang YZ, Gout PW. The xc– cystine/glutamate antiporter: a mediator of pancreatic cancer growth with a role in drug resistance. Br J Cancer. 2008 Aug 5;99(3):464–72.
18. Robert SM, Buckingham SC, Campbell SL, et al. SLC7A11 expression is associated with seizures and predicts poor survival in patients with malignant glioma. Sci Transl Med. 2015 May 27;7(289):289ra86.
19. Fogal B, Li J, Lobner D, McCullough LD, Hewett SJ. System x(c)– activity and astrocytes are necessary for interleukin-1 beta-mediated hypoxic neuronal injury. J Neurosci. 2007 Sep 19;27(38):10094–105.
20. Gout PW, Buckley AR, Simms CR, Bruchovsky N. Sulfasalazine, a potent suppressor of lymphoma growth by inhibition of the x(c)– cystine transporter: a new action for an old drug. Leukemia. 2001 Oct;15(10):1633–40.
21. Peppercorn MA. Sulfasalazine. Pharmacology, clinical use, toxicity, and related new drug development. Ann Intern Med. 1984 Sep;101(3):377–86.
22. Keystone EC, Wang MM, Layton M, Hollis S, McInnes IB; D1520C00001 Study Team. Clinical evaluation of the efficacy of the P2X7 purinergic receptor antagonist AZD9056 on the signs and symptoms of rheumatoid arthritis in patients with active disease despite treatment with methotrexate or sulphasalazine. Ann Rheum Dis. 2012 Oct;71(10):1630–5.
23. Rains CP, Noble S, Faulds D. Sulfasalazine. A review of its pharmacological properties and therapeutic efficacy in the treatment of rheumatoid arthritis. Drugs. 1995 Jul;50(1):137–56.
24. Zhang P, Liu Y, Jin C, Zhang M, Tang F, Zhou Y. Histone acetyltransferase GCN5 regulates osteogenic differentiation of mesenchymal stem cells by inhibiting NF-κB. J Bone Miner Res. 2016 Feb;31(2):391–402.
25. Liu Y, Zhao Y, Zhang X, et al. Flow cytometric cell sorting and in vitro pre-osteoinduction are not requirements for in vivo bone formation by human adipose-derived stromal cells. PLoS One. 2013;8(2):e56002.
26. Ducy P, Desbois C, Boyce B, et al. Increased bone formation in osteocalcin-deficient mice. Nature. 1996;382(6590):448–52.
27. Bouxsein ML, Boyd SK, Christiansen BA, Guldberg RE, Jepsen KJ, Muller R. Guidelines for assessment of bone microstructure in rodents using micro-computed tomography. J Bone Miner Res. 2010;25(7):1468–86.
28. Hinoi E, Takarada T, Uno K, Inoue M, Murafuji Y, Yoneda Y. Glutamate suppresses osteoclastogenesis through the cystine/glutamate antiporter. Am J Pathol. 2007 Apr;170(4):1277–90.
29. Kilberg MS, Shan J, Su N. ATF4-dependent transcription mediates signaling of amino acid limitation. Trends Endocrinol Metab. 2009 Nov;20(9):436–43.
30. McCauley LK. c-Maf and you won't see fat. J Clin Invest. 2010 Oct;120(10):3440–2.
31. Takada I, Kouzmenko AP, Kato S. Wnt and PPARγ signaling in osteoblastogenesis and adipogenesis. Nat Rev Rheumatol. 2009 Aug;5(8):442–7.
32. Kawai M, Rosen CJ. PPARγ: a circadian transcription factor in adipogenesis and osteogenesis. Nat Rev Endocrinol. 2010 Nov;6(11):629–36.
33. Uno K, Takarada T, Nakamura Y, Fujita H, Hinoi E, Yoneda Y. A negative correlation between expression profiles of runt-related transcription factor-2 and cystine/glutamate antiporter xCT subunit in ovariectomized mouse bone. J Pharmacol Sci. 2011;115(3):309–19.
34. Centrella M, Horowitz MC, Wozney JM, McCarthy TL. Transforming growth factor-beta gene family members and bone. Endocr Rev. 1994 Feb;15(1):27–39.
35. Hogan BL. Bone morphogenetic proteins in development. Curr Opin Genet Dev. 1996 Aug;6(4):432–8.
36. Panetta NJ, Gupta DM, Lee JK, Wan DC, Commons GW, Longaker MT. Human adipose-derived stromal cells respond to and elaborate bone morphogenetic protein-2 during in vitro osteogenic differentiation. Plast Reconstr Surg. 2010 Feb;125(2):483–93.
37. Wu G, Fang YZ, Yang S, Lupton JR, Turner ND. Glutathione metabolism and its implications for health. J Nutr. 2004 Mar;134(3):489–92.

38. Fratelli M, Goodwin LO, Ørom UA, et al. Gene expression profiling reveals a signaling role of glutathione in redox regulation. Proc Natl Acad Sci U S A. 2005 Sep 27;102(39):13998–4003.

39. Bräutigam L, Jensen LD, Poschmann G, et al. Glutaredoxin regulates vascular development by reversible glutathionylation of sirtuin 1. Proc Natl Acad Sci U S A. 2013 Dec 10;110(50):20057–62.

40. Takarada-Iemata M, Takarada T, Nakamura Y, Nakatani E, Hori O, Yoneda Y. Glutamate preferentially suppresses osteoblastogenesis than adipogenesis through the cystine/glutamate antiporter in mesenchymal stem cells. J Cell Physiol. 2011 Mar;226(3):652–65.

41. Maheshwari RA, Dhakwala F, Balaraman R, Seth AK, Soni H, Patel G. Maxcal-C (a polyherbal formulation) prevents ovariectomy-induced osteoporosis in rats. Indian J Pharmacol. 2015 Sep-Oct;47(5):555–9.

42. Zallot C, Billioud V, Frimat L, Faure P, Peyrin-Biroulet L; CREGG (Club de Reflexion des cabinets et Groupes d'Hépato-Gastroentérologie). 5-Aminosalicylates and renal function monitoring in inflammatory bowel disease: a nationwide survey. J Crohns Colitis. 2013 Aug;7(7): 551–5.

43. Plosker GL, Croom KF. Sulfasalazine: a review of its use in the management of rheumatoid arthritis. Drugs. 2005;65(13):1825–49.

44. Rubinstein A, Das KM, Melamed J, Murphy RA. Comparative analysis of systemic immunological parameters in ulcerative colitis and idiopathic proctitis: effects of sulfasalazine in vivo and in vitro. Clin Exp Immunol. 1978 Aug;33(2):217–24.

45. Delamere JP, Farr M, Grindulis KA. Sulphasalazine induced selective IgA deficiency in rheumatoid arthritis. Br Med J (Clin Res Ed). 1983 May 14;286(6377):1547–8.

46. Wittenberg HR, Kleemeyer K, Hoppe U, Peskar BM, Peskar BA. Release of eicosanoids from human synovial tissue and the effect of anti-inflammatory drugs. Prog Clin Biol Res. 1987;242:277–82.

47. Chung WJ, Lyons SA, Nelson GM, et al. Inhibition of cystine uptake disrupts the growth of primary brain tumors. J Neurosci. 2005 Aug 3;25(31):7101–10.

48. Robe PA, Bentires-Alj M, Bonif M, et al. In vitro and in vivo activity of the nuclear factor-kappaB inhibitor sulfasalazine in human glioblastomas. Clin Cancer Res. 2004 Aug 15;10(16):5595–603.

49. Nie S, Xu J, Zhang C, Xu C, Liu M, Yu D. Salicortin inhibits osteoclast differentiation and bone resorption by down-regulating JNK and NF-kappaB/NFATc1 signaling pathways. Biochem Biophys Res Commun. 2016 Jan 29;470(1):61–7.

50. Jimi E, Fukushima H. [NF-kappaB signaling pathways and the future perspectives of bone disease therapy using selective inhibitors of NF-kappaB]. Clin Calcium. 2016 Feb;26(2):298–304. Japanese

51. Lorenzo J, Horowitz M, Choi Y. Osteoimmunology: interactions of the bone and immune system. Endocr Rev. 2008 Jun;29(4):403–40.

52. Khosla S. Minireview: the OPG/RANKL/RANK system. Endocrinology. 2001 Dec;142(12):5050–5.

53. Sykes L, Thomson KR, Boyce EJ, et al. Sulfasalazine augments a pro-inflammatory response in interleukin-1beta-stimulated amniocytes and myocytes. Immunology. 2015 Dec;146(4):630–44.

54. Habens F, Srinivasan N, Oakley F, Mann DA, Ganesan A, Packham G. Novel sulfasalazine analogues with enhanced NF-kB inhibitory and apoptosis promoting activity. Apoptosis. 2005 May;10(3):481–91.